Available online at www.sciencedirect.com
ScienceDirect
Catalysis Today 133–135 (2008) 639–646
CATALYSIS TODAY
www.elsevier.com/locate/cattod

The influence of Ti-loading on the acid behavior and on the catalytic efficiency of mesoporous Ti-MCM-41 molecular sieves

Griselda A. Eimer, Sandra G. Casuscelli, Corina M. Chanquia, Verónica Elías, Mónica E. Crivello, Eduardo R. Herrero *

Centro de Investigación y Tecnología Química (CITeQ), Universidad Tecnológica Nacional, Facultad Regional Córdoba, Maestro Lopez esq., Cruz Roja Argentina (5016), Córdoba, Argentina

Available online 19 February 2008

Abstract

Ti-containing mesoporous catalysts with MCM-41 structure and high surface area have been successfully prepared by direct hydrothermal synthesis. Various techniques including XRD, DRUV–vis, ICP, N_2 adsorption and absorption of pyridine coupled to IR spectroscopy are employed. A detailed study about the relationships existing between the Ti loading in the catalyst, the acid properties and the catalytic efficacy is presented in this contribution. The incorporation of titanium into the silica framework provoked mainly a proportional increase of Lewis acid sites. However, Bronsted acid sites were also generated at high Ti loadings. Whereas the Lewis sites are related with presence of tetrahedral Ti species in the framework, the Bronsted sites would be generated by the vicinity of these Ti species to the structure SiOH groups. The oxidation of cyclohexene with aqueous hydrogen peroxide was employed as a test reaction to evaluate the activity and effectiveness of the active sites. We could corroborate that the Ti sites were active and available even at high Ti loadings. The reaction presented a high velocity during the 1st hours and afterwards it could not continue evolving due to the almost total peroxide consumption. Cyclohexene epoxide was the main product from reaction.

Keywords: Ti-MCM-41; Mesoporous materials; M41S; Surface acidity; Epoxidation; Cyclohexene; Pyridine absorption

1. Introduction

Mesoporous molecular sieves of the MCM-41 type possess a hexagonal packed array of channels with narrow pore-size distributions [1–3]. These materials have many potential applications in the pharmaceutical and fine chemical industries, petroleum refining, adsorption and separation processes and heterocatalysis, mostly owing to their large specific surface area of up to 1000 m^2/g and controlled pore dimensions with uniform pore-size distribution. The catalytic properties of molecular sieves rely on the presence of active sites in their frameworks. In the case of MCM-41, the incorporation of heteroatoms to the otherwise electrically neutral purely siliceous framework may generate active sites. Thus, the introduction of titanium in MCM-41 results of great interest in oxidation reactions especially of large molecules which cannot diffuse in the pores of microporous materials [4–8]. Since in the industrial manufacturing of fine chemicals the selective oxidation transformations are still widely performed by means of large amounts of organic peroxoacids and of transition metal reagents, the use of titanosilicate-based heterogeneous catalysts may contribute remarkably to the set-up of environmentally benign industrial processes. On the other hand, dilute hydrogen peroxide is one of the most convenient oxidants due to its easy handling, high content of active oxygen and absence of by-products [9]. In this context, the selective oxidation of organic compounds, and especially of the bulky olefinic compounds, over Ti-based catalysts and H_2O_2 has gained considerable interest. Moreover, the synthesis of large pore titanium-containing catalysts such as mesoporous Ti-MCM-41 have opened new routes to catalytic oxidation of bulky molecules and the synthesis of new products [4–12]. Consequently, for the application of MCM-41 in catalysis, a detailed knowledge concerning the acid sites of these materials is desirable. Even though the active sites existing in the mesopores of the titanium-containing MCM-41 were investigated earlier by different spectroscopic techniques [13–15], many questions have remained open and their chemical strength and nature

* Corresponding author.
E-mail address: eherrero@scdt.frc.utn.edu.ar (E.R. Herrero).

0920-5861/$ – see front matter © 2007 Elsevier B.V. All rights reserved.
doi:10.1016/j.cattod.2007.12.096

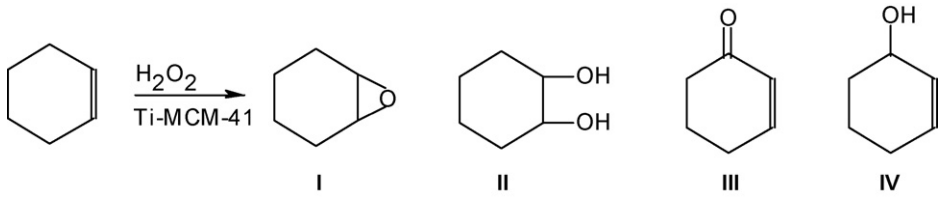

Scheme 1. Oxidation of cyclohexene with hydrogen peroxide catalyzed by Ti-MCM-41. The desired product is cyclohexene oxide (**I**), and the potential side products are 1,2-cyclohexanediol (**II**), 2-cyclohexen-1-one (**III**) and 2-cyclohexen-1-ol (**IV**).

continues even under discussion. The oxidation of cyclohexene using hydrogen peroxide is frequently used as a test reaction for the catalytic evaluation of different titanium-modified materials. Scheme 1 illustrates some of the typical products of cyclohexene oxidation. The cyclohexene oxide (I), generated by the heterolytic epoxidation of the cyclohexene double bond, and the 1,2-cyclohexanediol (II) side product, formed by hydrolysis of the epoxide ring, generally reflect a concerted process. In contrast, the allylic oxidation side products, 2-cyclohexen-1-one (III) and 2-cyclohexen-1-ol (IV), are often ascribed to a homolytic radical pathway [16,17]. Various authors have studied the catalytic performance of Ti-MCM-41 catalysts in the oxidation reaction of cyclohexene, reporting a low catalytic activity and epoxide selectivity [17–20]. On the other hand, although different metal loadings in the catalyst may induce changes in the surface species and may modify, sometimes noticeably, the catalytic features, little research has been done for elucidating the effect of varying the titanium content on the catalytic effectiveness of the active sites.

The aim of the present work was to study the influence of the Ti loading in a series of MCM-41 materials, prepared by hydrothermal synthesis, over their acid properties and active sites efficiency. The surface acidity was monitored by using in situ FT-IR of pyridine adsorption. The catalytic properties of Ti-MCM-41 were tested for the cyclohexene oxidation reaction with H_2O_2 and rate constants per active site were calculated.

2. Experimental

The titanium-containing mesoporous catalysts, having various Si/Ti atomic ratios, were synthesized according to the procedure described by us elsewhere [21]. These materials were characterized by ICP, XRD, DRUV–vis and N_2 adsorption according to the Ref. [21]. Prior to the specific surface area measurements, samples were out gassed at 400 °C under N_2 flow for 2 h. Density functional theory (DFT) method was applied to evaluate the pore-size distribution [22].

2.1. Acidity measurements

To evaluate and analyze the strength and type of acid site, FTIR spectral measurements of pyridine adsorption on the samples were performed on a JASCO 5300 spectrometer through the following procedure. A self-supporting wafer for each sample (~20 mg/cm^2) was prepared, placed in a thermostatized cell with CaF_2 windows connected to a vacuum line and evacuated for 8 h at 400 °C. The background spectrum was recorded first after cooling the sample to room temperature. Afterwards, the solid wafer was exposed to pyridine vapors at room temperature and allowed to saturate for 20 min. The IR spectrum for each sample was obtained after pyridine desorption by evacuation for 1 h at 200, 300 and 400 °C. The difference spectrum was obtained finally by subtracting the background spectrum recorded previously.

2.2. Catalytic experiments

The cyclohexene oxidation reactions with H_2O_2 were carried out at 70 °C under stirring in 2-ml glass vials immersed in a thermostated bath. Typically, the reaction mixture for each vial, consisted of 9.00 mg of catalyst, 91.90 mg of cyclohexene (Baker ≈98%), 26.60 mg of oxidant (hydrogen peroxide 35%, w/w, Riedel-de Haen) and 678.30 mg of solvent (acetonitrile, Cicarelli). Such reaction mixture was placed in different vials corresponding to different sampling times. In all cases, the oxidant to substrate molar ratio was 1:4. Vials were withdrawn at different times and analyzed by gas chromatography (Hewlett Packard 5890 Series II) using a capillary column (cross-linked methyl–silicone gum, 30-m long) and flame ionization detector. Additionally, the GC–MS (Shimadzu-QP 5050 A) analyses were performed in order to identify the reaction products. The total conversion of H_2O_2 was measured by iodometric titration. The cyclohexene conversion, named X_C, was defined as the ratio of converted species to initial concentration. In order to examine the effect of the Ti loading in the catalyst over the efficacy of the active sites, the reaction rate constants were calculated for the different Ti contents.

3. Results and discussion

Table 1 summarizes the chemical composition and structural properties of the different catalysts prepared in this study. The XRD patterns, reported by us elsewhere [21], were typical of MCM-41 structure. No diffraction peaks in the region of higher angles (10–50°) could be observed, thus indicating the absence of bulk anatase in the samples and suggesting that Ti-MCM-41 sample is a pure phase. All the samples showed great surface areas which ranged from approximately 1400 to 2000 m^2/g. The decreasing specific surface area with the Ti content may be correlated to the decrease in the structural order, as observed in the XRD patterns. Consequently, an increasing amount of transition metal could obstruct the structure-directing action of template and result in the formation of partially broken pores as well as a lower surface area. On the other hand, the pore

Table 1
Chemical composition and structural properties for the Ti-MCM-41 catalysts with different Ti contents and the corresponding pure silica MCM-41

Sample	Si/Ti[a] (molar ratio)	Ti content[b] (wt.%)	a_0 (Å)	Surface area (m^2/g)	d_{DFT} [c] (Å)
Ti-MCM-41(20)	20	2.50	38.48	1447	28.50
Ti-MCM-41(30)	30	2.00	38.11	1490	27.52
Ti-MCM-41(40)	40	1.54	37.22	1541	27.24
Ti-MCM-41(60)	60	1.12	36.28	1546	27.25
Ti-MCM-41(120)	120	0.59	36.14	1620	25.78
Ti-MCM-41(234)	234	0.25	36.11	1738	25.49
Si-MCM-41	∞	0.00	36.09	2040	25.24

[a] In synthesis gel.
[b] In final solid product.
[c] Pore diameter corresponding to the maximum of the pore-size distribution obtained by the DFT method.

diameters increase slightly when increasing Ti loadings. A DRUV–vis spectroscopy analysis, as shown in our previous paper [21], allowed us to infer that most of the active Ti sites are isolated and in tetrahedral (Td) coordination in MCM-41 framework and that anatase phase is absent in all the cases.

The chemisorption of pyridine followed by IR studies is usually a useful probe to detect the presence and nature of surface aprotic (Lewis) acid and protonic (Bronsted) acid sites on a catalyst surface [23]. It is well known that pyridine, as basic molecule, can interact via the nitrogen lone-pair electrons with these acid sites, giving rise to characteristic bands. Information on the strength of Lewis and Bronsted acid sites can be obtained from pyridine thermodesorption. Here, the surface acidity of various samples was measured using the well-established pyridine adsorption technique. Fig. 1 shows a set of in situ FT-IR spectra of the catalysts recorded after the adsorption of pyridine and subsequent evacuation at 200, 300 and 400 °C. All the samples show bands corresponding to hydrogen-bonded pyridine at 1447 and 1599 cm^{-1} [14,15,24–26]. These are the only bands found in pure Si-MCM-41 which decreased sharply upon evacuation at elevated temperature. Thus pyridine would form hydrogen bonds with the silanol groups present in the structure whose hydroxyls are not capable to protonate pyridine. In concordance, Otero Areán et al. [27] assigned the band at 1596 cm^{-1} in gallia–silica samples to Bronsted-acid sites which were not strong enough to protonate pyridine but which could form hydrogen-bonded adducts.

According to the literature, the formation of Lewis-type adducts with adsorbed pyridine is typically identified by IR absorption bands at about 1445–1460, 1575–1580 and 1600–1620 cm^{-1} [14,15,24–29]. As observed in Fig. 1, the titanium-containing MCM-41 catalysts show a band at 1608 cm^{-1} corresponding to pyridine coordinately bonded to Lewis acid sites [14,15,24–28]. This band is increased proportionally according to the amount of titanium incorporated into the catalysts. Moreover, the systematic increase of the IR absorption band at 1447 cm^{-1} with growing Ti content could be interpreted in terms of the overlapping of both the hydrogen-bonded pyridine band (1447 cm^{-1}) and a band attributed to a Lewis-type adduct which frequently appears at 1450 cm^{-1}

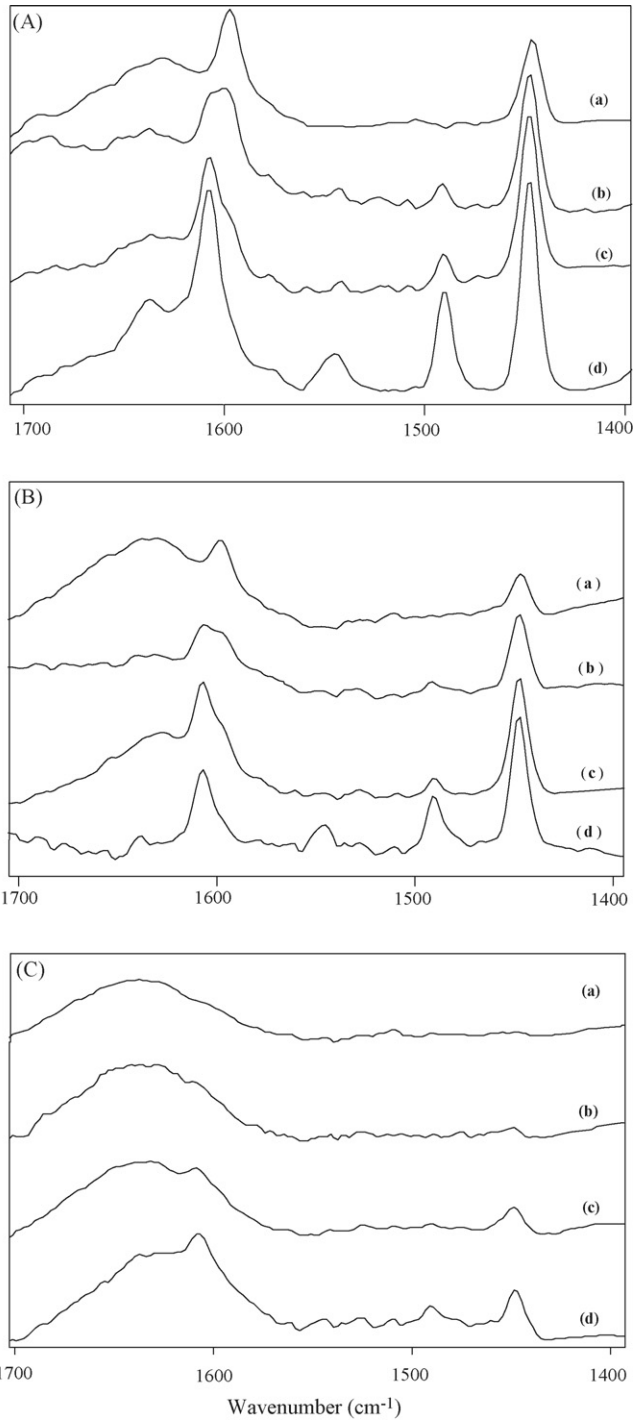

Fig. 1. FTIR of pyridine adsorbed on the samples: (a) Si-MCM-41, (b) Ti-MCM-41(120), (c) Ti-MCM-41(60) and (d) Si-MCM-41(20), after desorption at 200 °C (A), 300 °C (B) and 400 °C (C).

[25]. A slight band at 1577 cm^{-1} due to pyridine coordinated to weak surface Lewis acid sites was also observed for all the Ti-MCM-41 samples [15].

Taking into account that sample wafers had approximately the same weight and surface density, a semi-quantitative estimation allowed us to suggest that the incorporation of titanium into the silica framework generates Lewis acid sites on the surface which increase with increasing titanium content.

These sites can be mainly attributed to the presence of coordinatively unsaturated surface exposed Ti^{4+} sites (tetrahedral-coordinated framework titanium).

On the other hand, all the titanium-containing samples exhibit a band at 1540 cm^{-1} which is remarkably more intense for the Ti-MCM-41(20) sample. Moreover, a band at 1636 cm^{-1} can be clearly observed for this sample with the highest titanium content. According to the literature, these latter bands distinctively identify the pyridinium ion [27,30–32]. Similarly to other metal-substituted mesoporous silica [27,32–34] we can assume that the incorporation of titanium gives rise to a small amount of Bronsted acid sites on the surface which are strong enough to protonate adsorbed pyridine. However, under evacuation at different temperatures these bands tend to disappear, indicating that the Bronsted sites are of a weak character. One of the possible origins of the generation of Bronsted acid sites on the Ti-MCM-41 material with high Ti content could be the weakness of the strength of the SiO–H bonds due to the presence of Ti^{4+} ions in the vicinity of the silanol groups existent in the structure [21]. When the smaller Si^{4+} ions are replaced by the larger Ti^{4+} ion in the framework of the solid, the bond length of Ti–O–Si clearly differs from the one of Si–O–Si which leads to some structure deformation evidenced by the XRD patterns. Moreover, Ti^{4+} ions in the vicinity of the hydroxyls carrying silicon could cause changes in the electron density around Si due to differences in electronegativity or to the local structure deformations resulting from the introduction of the titanium into the framework, thus weakening the SiO–H bonds [32,35]. In addition, a band corresponding to vibration of pyridine associated with both, Lewis and Bronsted acid sites, was observed at 1490 cm^{-1}. On the other hand, taking into account the relative intensity of the bands associated with the Lewis and Bronsted acid sites, the Lewis acidity resulted more important. As the heating temperature reached 300 °C under vacuum (Fig. 1B), the intensities of all the bands slightly lowered. After desorption at 400 °C, these bands underwent a further reduction for the Ti-MCM-41 samples. However, on the Si-MCM-41 sample, all the bands completely disappeared at 400 °C, indicating that the interaction between pyridine and the pure Si-MCM-41 structure is weaker and thus the acid strength. Moreover, considering that the hydrogen-bonded pyridine bands intensity decreases drastically at 400 °C (Fig. 1B(d)), the presence of the band at 1447 cm^{-1} at this temperature for the Ti-MCM-41 samples provides clear evidence that the same has a contribution from Lewis acid sites which are strong enough to retain the pyridine molecules until 400 °C.

Fig. 2 shows the IR spectra in the hydroxyl range of Ti-MCM-41(20) and Ti-MCM-41(60) before and after pyridine adsorption followed by desorption at 200 °C. Only a very intense band at 3740 cm^{-1} was observed for all the samples and attributed to non-interacting and non-acidic (Si–OH) silanol groups [14,21,24,32]. The intensity of this band does not change significantly upon pyridine adsorption, indicating a high residual concentration of OH groups on all the samples. However, a slight reduction and broadening of the same could evidence the interactions existing between hydrogen and

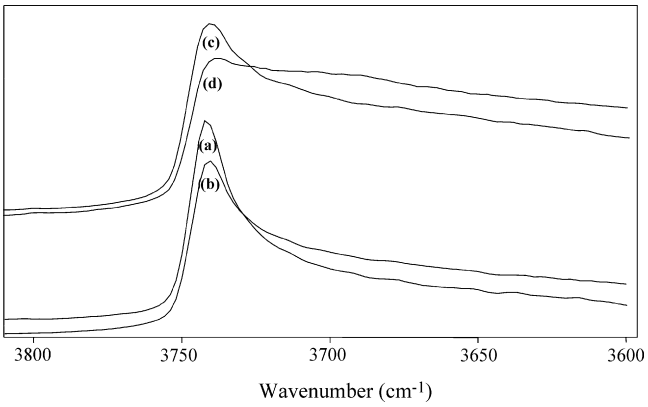

Fig. 2. FTIR in the hydroxyl region of catalysts Ti-MCM-41(60): (a) before pyridine adsorption, (b) after pyridine adsorption and desorption at 200 °C and Ti-MCM-41(20): (c) before pyridine adsorption and (d) after pyridine adsorption and desorption at 200 °C.

pyridine. Note that the hydroxyl region of these calcined samples does not show the presence of the IR bands at approximately 3615 and 3665 cm^{-1}, which are characteristic of acid sites. This does not mean that these samples do not contain acid sites since the pyridine region shows the presence of as many Lewis sites as Bronsted sites (silanol groups with an enhanced acid strength).

In a previous study we have demonstrated [21] that the different physicochemical techniques indicate that the titanium was incorporated into the silica framework in all the Ti-MCM-41 samples prepared and these framework Ti(IV) species are the effective active sites for the selective oxidation of cyclohexene with aqueous hydrogen peroxide. The catalysts synthesized here showed a very good activity for the epoxidation of cyclohexene, being the cyclohexene oxide (**I**) the main reaction product in almost the whole range of Ti loadings on the catalysts studied. The formation of 1,2-cyclohexanediol (**II**) as by-product arising from epoxide ring-opening reactions and allylic oxidation side reactions were also observed. The yield to the different reaction products, shown in Fig. 8, is discussed below.

Fig. 3 shows the cyclohexene conversion profiles versus the reaction time for the different catalysts synthesized. The conversion increased strongly in the 1st reaction hour and then a dramatic slope change, which is more accentuated in the catalyst with higher Ti content, was observed. Therefore, this reaction, which was initially very fast, shows a general tendency to stop after the 1st hour. On the other hand, Fig. 4 shows the amount of H_2O_2 consumed (mmol) in function of reaction time for the different catalysts. As it can be seen, the reaction is fast and most of the hydrogen peroxide is consumed in the 1st hours. The relatively high amount of titanium accounts for the fastest reaction and it is noteworthy that the peroxide conversion was approximately 86% in the 1st hour for the catalyst with higher Ti loading. Thus, since the described reaction was carried out with an excess of alkene, the observed cyclohexene conversion profiles could be attributed to a fast consumption of the limiting reactant (peroxide) at the beginning of the reaction. Another possibility could be the

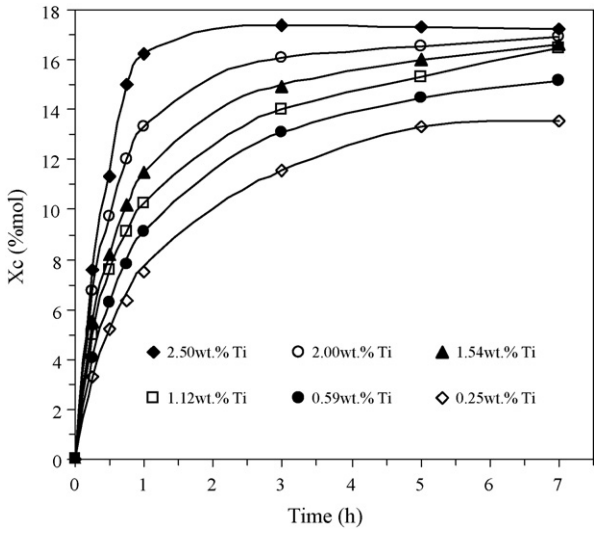

Fig. 3. Cyclohexene conversion vs. reaction time on Ti-MCM-41 catalysts with different Ti contents. Reaction conditions: cyclohexene/H_2O_2 (mol/mol) = 4; catalyst = 9.79 wt.% of the substrate; temperature: 70 °C.

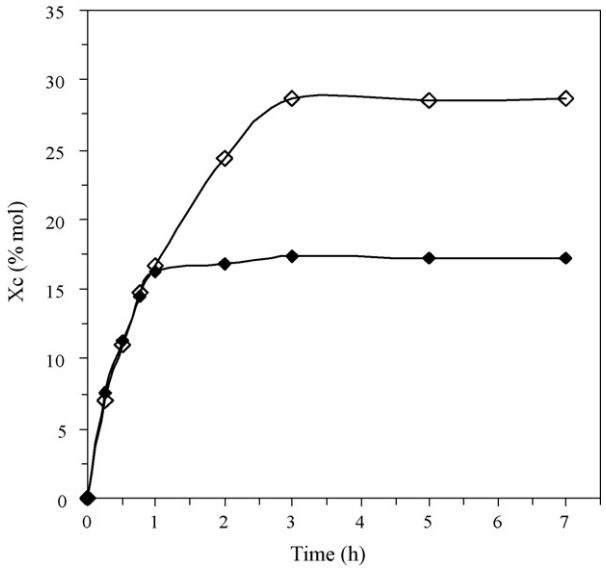

Fig. 5. Cyclohexene conversion vs. reaction time on Ti-MCM-41(20) (2.00 wt.% of Ti). (◆) Without addition of peroxide and (◇) with addition of peroxide.

deactivation of the catalyst with the reaction time due to the adsorption of by-products onto the catalyst surface. It is known that some by-products, such as the glycols, can be coordinated to titanium thereby blocking these centers from further reactants [18]. To check this possible poisoning of the active sites, we carried out an experiment in which an amount of H_2O_2 was added to the reaction medium after the 1st hour in order to recover its initial concentration. The results of this experience using the catalyst Ti-MCM-41(20) are shown in Fig. 5. As it can be seen, the conversion increased approximately 60% after the H_2O_2 addition, indicating that there were active sites still available for the reaction. This suggests that the Ti sites are not deactivated by the adsorption of by-products onto the catalyst surface under our reaction conditions, corroborating that the reaction would not continue evolving due to very high consumption of the H_2O_2 during the 1st hours of the reaction. However, it can also be observed in Fig. 3 that the catalytic activity at 7 reaction hours increases with the Ti content but, above a 1 wt.% loading, the conversion values basically keep unchanged. Then, although the DRUV–vis spectra of the samples show that the actual number of active tetrahedral Ti sites increases proportionally to the increase in Ti loading, this fact does result in an increase of activity above a 1 wt.% Ti loading. Again, this could induce us to believe that many of the Ti sites in the catalysts with higher loadings can be deactivated and not be effectively used. Other possible explanation could also be that, Ti–O–Ti bridges can be formed for relatively high loadings, as it is evidenced by the broadening of the main UV–vis band, and these will not display the same catalytic activity. To clarify this point, the influence of the Ti loading over the effectiveness of the active sites has been studied. In order to determine the reaction rate constant values for all the catalysts with different Ti contents, we performed a fitting of the catalytic data using a pseudohomogenous model.

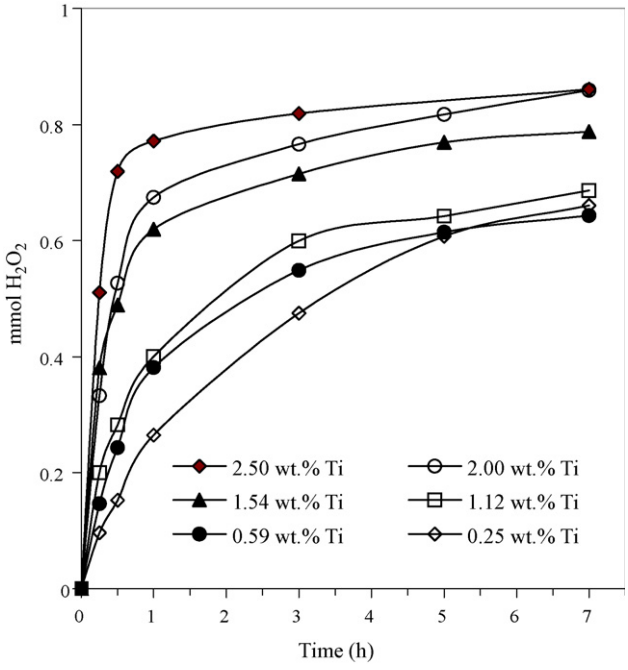

Fig. 4. Amount of H_2O_2 consumed (mmol H_2O_2) through the reaction time for the different catalysts.

Taking into account the similarity of our reaction system ($C_6H_{10} + H_2O_2 \rightarrow$ products, using Ti-MCM-41 as catalyst) with the oxidation of other cyclic olefin whose rate law was experimentally found by us under the same conditions [8], we consider that the following expression can be used:

$$-r_{C_6H_{10}} = -\frac{d[C_6H_{10}]}{dt} = k[cat][C_6H_{10}][H_2O_2]$$

Taking into account that the cyclohexene conversions (X_C) versus reaction time for the different catalysts were the

experimental data, the above equation can be written as

$$-r_{C_6H_{10}} = -\frac{dX_C}{dt} = k[cat][C_6H_{10}]_0(1 - X_C)(M - X_C)$$

where $M = [H_2O_2]_0/[C_6H_{10}]_0$, $_0$ = [initial].

These differential equations were numerically integrated by using the Runge–Kutta–Merson algorithm. The model parameters estimation was performed by non-linear regression, which minimizes the objective functions $Q = \sum(X_{Cj} - X_{C*j})$, where X_C and X_{C*} are the experimental and calculated conversions, respectively, and j the reaction time.

Considering that, in the case of catalyst with the highest Ti loading, the studied reaction is practically stopped after the 1st hour (Figs. 3 and 4) and, in order to analyze all the catalysts in the same range of reaction times, we show the experimental data fitted during the 1st reaction hour (Fig. 6).

The rate constants obtained at 70 °C for all the different catalysts are given in Table 2. Fig. 7 shows the rate constant (k) and the ratio between this constant and the Ti moles number per catalyst gram (k/Ti) in terms of the Ti content in the catalyst. The k increases proportionally with the Ti content, while k/Ti initially decreases and then basically keeps unchanged with growing Ti loading. The high k value per Ti site at lower Ti content would indicate a high dispersion of the active species in the material. Consequently, a relatively small amount of Ti incorporated in the MCM-41 framework leads to evenly dispersed and isolated active Ti sites, which show the highest catalytic effectiveness. When Ti loading is more than 1 wt.%, k/Ti remains unchanged indicating that the sites individual effectiveness is not affected by an increase of metal content in the catalyst. In contrast with our belief and, if we take into account that the active sites are not blocked due to the by-products adsorption, the above finding allows us to suggest that all the sites remain active and available even in the case of catalysts with higher Ti contents. Moreover, although the presence of Ti–O–Ti bonds cannot be discarded by UV–vis for the relatively high Ti loadings, the effect of these species on the catalytic activity was not observed since, as it was analyzed above, the effectiveness per active site remains constant even for high Ti loadings. Then, the fact that the increase in Ti loading above 1 wt.% does not result in an increase of activity at 7 h could be also attributed to the high initial reaction rate which causes that most of the limiting reactant is consumed during the 1st hours, not allowing the reaction to follow.

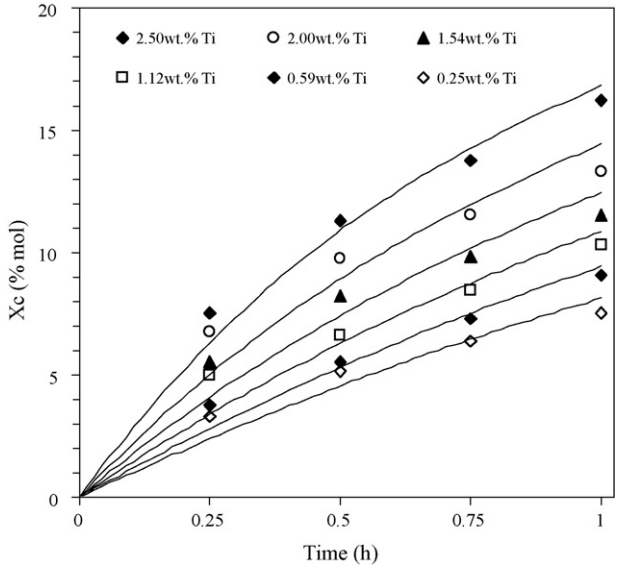

Fig. 6. Fitting of experimental data of cyclohexene conversion vs. reaction time during the 1st hour on the different Ti-MCM-41 catalysts synthesized. Points: experimental results; solid lines: model predictions.

Table 2
Kinetic parameters of cyclohexene oxidation with H_2O_2 over Ti-MCM-41 catalysts determined by modeling experimental data

Sample	Kinetic constants (k)[a]	S.D.
Ti-MCM-41(20)	0.11986	$\pm 6.3 \times 10^{-3}$
Ti-MCM-41(30)	0.09149	$\pm 5.2 \times 10^{-3}$
Ti-MCM-41(40)	0.07255	$\pm 4.5 \times 10^{-3}$
Ti-MCM-41(60)	0.05593	$\pm 3.8 \times 10^{-3}$
Ti-MCM-41(120)	0.04302	$\pm 3.2 \times 10^{-3}$
Ti-MCM-41(234)	0.04158	$\pm 3.6 \times 10^{-3}$

[a] Intervals calculated with 99% of confidence; $R^2 = 0.99$.

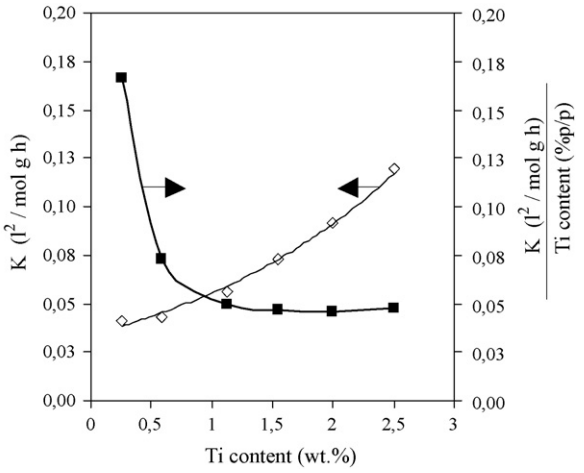

Fig. 7. Rate constant (k) (□) and ratio (■) between this constant and the Ti moles number per catalyst gram (k/Ti) in terms of the Ti content in the catalyst.

Fig. 8 shows the influence of the amount of Ti incorporated in the MCM-41 framework over the products yield for the cyclohexene oxidation reaction with H_2O_2. The epoxide is the main reaction product and its yield increases with growing Ti load up to reaching the maximum level when Ti content is about 1–1.5 wt.%. As it is evidenced by the pyridine adsorption–desorption measurements followed by FT-IR, the introduction of Ti into the MCM-41 framework generates Lewis acid sites onto the catalyst surface. They can act as traps for electron-donor molecules and participate in the oxygen transfer which occurs in the selective oxidation reactions. It is now established that the active catalytic species in the epoxidation reactions with hydrogen peroxide over Ti-containing zeolites is a complex containing a hydroperoxo ligand [36]. The nucleophilic attack of the double bond of the alkene on an oxygen atom of such a complex leads to the epoxide formation. For higher Ti content, the epoxide selectivity decreases steadily due to an opening side reaction of epoxide ring with water, probably

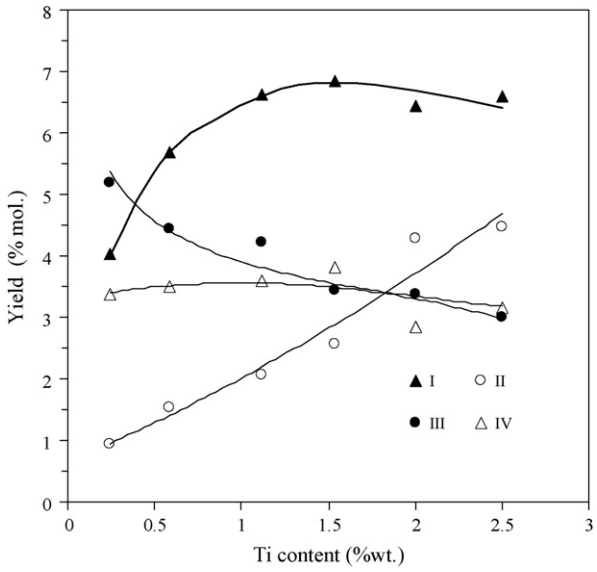

Fig. 8. Influence of Ti content on Ti-MCM-41 on the yield to reaction products for the cyclohexene oxidation using H_2O_2 as oxidant.

catalyzed by the acid character of the titanosilicates. It should be taken into account that, as it has been observed by the broadening of the main UV–vis band of the catalyst at higher Ti contents [21], H_2O has a strong tendency to coordinate with the four coordinated Ti species. Moreover, the Lewis acid sites of catalyst, being the active species for the epoxidation [21], can also coordinate to water molecules which may react with the formed epoxide via epoxide ring-opening reactions leading to the formation of 1,2-cyclohexanediol as side product. On the other hand, the IR spectra of adsorbed pyridine over the catalysts with higher Ti loading reveal the presence of Bronsted acid sites which could also be responsible for the higher opening of the epoxide ring to form glycol when the Ti content in the catalyst increases. However, it is very important to note that, in contrast with other results [17–20], the epoxide is our main reaction product on Ti-MCM-41 along almost the whole range of Ti contents studied. Furthermore, the Ti hydroperoxy sites of the above mentioned complex can undergo a homolytic cleavage of the O–O bond leading to the allylic oxidation reaction [16]. The products arising from this reaction are observed in a low extent being unfavored by the increasing Ti content in the MCM-41 structure.

4. Conclusions

A series of Ti-containing mesoporous catalysts has been prepared and characterized. The influence of the Ti loading on the structural, acid and catalytic properties of these materials has been studied. In all the cases, solids with high specific surface area and structure typical of MCM-41 materials were obtained. The Ti species were mainly located in the framework in tetrahedral positions. The FT-IR spectra of adsorbed pyridine revealed that the incorporation of Ti into the mesostructure generates mainly Lewis acid sites onto the surface; however it was also possible to detect Bronsted acid sites for the catalysts with higher Ti loading. The Bronsted acidity could be attributed to the weakness of the strength of the SiO–H bonds due to the presence of Ti^{4+} ions in the vicinity of the structure silanol groups. The Lewis acidity would arise from the coordinatively unsaturated Ti^{4+} sites present in the framework. The materials synthesized showed very good activity for the selective oxidation of cyclohexene using H_2O_2 as oxidant. This reaction shows a high initial rate and seems to stop after the 1st hour due to the low residual concentration of peroxide in the reaction medium. This fact could be corroborated by the increase in the conversion observed when H_2O_2 was added during the reaction development. In this way, the deactivation of catalyst with increasing reaction time due to blocking of the active sites by adsorbed by-products can be discarded. The calculation of the rate constants per site allowed us to determine that the efficacy of the active sites is not affected by the high Ti loadings. Thus, it is possible to suggest that the Ti sites remain active and available even though high contents of Ti are incorporated into the catalyst. The main oxidation product was the cyclohexene oxide, indicating that the direct epoxidation mechanism which takes place through the formation of the metal-hydroperoxo intermediary is being favored.

Acknowledgements

G.A.E. and S.G.C. CONICET Researchers; C.M.Ch. and V.R.E. CONICET Doctoral Fellowships. This work was supported by the CONICET and the UTN-FRC of Argentina. The authors thank geol. Julio D. Fernández (UTN-FRC, Córdoba, Argentina) for help in recording FT-IR data.

References

[1] C. Kresge, M. Leonowicz, W. Roth, J. Vartuli, J. Beck, Nature 359 (1992) 710.
[2] J. Vartuli, K. Schmidt, C. Kresge, W. Roth, M. Leonowicz, S. McCullen, S. Hellring, J. Beck, J. Schlenker, D. Olson, E. Sheppard, Chem. Mater. 6 (1994) 2317.
[3] J. Beck, C. Chu, I. Jonson, C. Kresge, M. Leonowicz, W. Roth, J. Vartuli, WO 91, 1991, 11390.
[4] C. Berlini, M. Guidotti, G. Moretti, R. Psaro, N. Ravasio, Catal. Today 60 (2000) 219.
[5] C. Berlini, G. Ferraris, M. Guidotti, G. Moretti, R. Psaro, N. Ravasio, Micropor. Mesopor. Mater. 44–45 (2001) 595.
[6] J. Gallo, I. Paulino, U. Schuchardt, Appl. Catal. A: Gen. 266 (2004) 223.
[7] M. Guidotti, N. Ravasio, R. Psaro, G. Ferraris, G. Moretti, J. Catal. 214 (2003) 242.
[8] M. Cagnoli, S. Casuscelli, A. Alvarez, J. Bengoa, N. Gallegos, N. Samaniego, M. Crivello, G. Ghione, C. Perez, E. Herrero, S. Marchetti, Appl. Catal. A: Gen. 287 (2005) 227.
[9] W. Sanderson, Pure Appl. Chem. 72 (2000) 1289.
[10] I. Arends, R. Sheldon, M. Wallau, U. Schuchardt, Angew. Chem. Int. Ed. Engl. 36 (1997) 1144.
[11] B. Notari, Adv. Catal. 41 (1996) 253.
[12] J. van der Waal, M. Rigutto, H. Van Bekkum, Appl. Catal. A 167 (1998) 331.
[13] M. Hunger, U. Schenk, M. Breuninger, R. Glaser, J. Weitkamp, Micropor. Mesopor. Mater. 27 (1998) 261.
[14] D. Trong On, S. Nguyen, V. Hulea, E. Dumitriu, S. Kaliaguine, Micropor. Mesopor. Mater. 57 (2003) 169.
[15] D. Srinivas, R. Srivastava, P. Ratnasamy, Catal. Today 96 (2004) 127.
[16] K. Balkus Jr., A. Khanmamedova, J. Shi, Stud. Surf. Sci. Catal. 110 (1997) 999.

[17] R. Sever, R. Alcala, J. Dumesic, T. Root, Micropor. Mesopor. Mater. 66 (2003) 53.
[18] A. Hagen, K. Schueler, F. Roessner, Micropor. Mesopor. Mater. 51 (2002) 23.
[19] L. Chen, G. Chuah, S. Jaenicke, Catal. Lett. 50 (1998) 107.
[20] S. Laha, R. Kumar, Micropor. Mesopor. Mater. 53 (2002) 163.
[21] G. Eimer, S. Casuscelli, G. Ghione, M. Crivello, E. Herrero, Appl. Catal. A: Gen. 298 (2006) 232.
[22] S. Gregg, K. Sing, Adsorption, Surface Area and Porosity, Academic Press, 1982.
[23] Parry, J. Catal. 2 (1963) 371.
[24] B. Chakraborty, B. Viswanathan, Catal. Today 49 (1999) 253.
[25] A. Sakthivel, S. Dapurkar, N. Gupta, S. Kulshreshtha, P. Selvam, Micropor. Mesopor. Mater. 65 (2003) 177.
[26] T. Conesa, J. Hidalgo, R. Luque, J. Campelo, A. Romero, Appl. Catal. A: Gen. 299 (2006) 224.
[27] C. Otero Areán, M. Rodriguez Delgado, V. Montouillout, J. Lavalley, C. Fernandez, J. Cuart Pascual, J. Parra, Micropor. Mesopor. Mater. 67 (2004) 259.
[28] L. Cedeño, D. Hernandez, T. Klimova, J. Ramirez, Appl. Catal. A: Gen. 241 (2003) 39.
[29] G. Turnes Palomino, J. Cuart Pascual, M. Rodríguez Delgado, J. Bernardo Parra, C. Otero Areán, Mater. Chem. Phys. 85 (2004) 145.
[30] E. Escalona Platero, M. Peñarroya Mentruit, C. Otero Areán, A. Zecchina, J. Catal. 162 (1996) 268.
[31] C. Morterra, G. Magnacca, Catal. Today 27 (1996) 497.
[32] L. Chen, L. Noreña, J. Navarrete, J. Wang, Mater. Chem. Phys. 97 (2–3) (2006) 236.
[33] H. Kosslick, G. Lischke, G. Walther, W. Storek, A. Martin, R. Fricke, Micropor. Mater. 9 (1997) 13.
[34] A. Infantes-Molina, J. Mérida-Robles, P. Maireles-Torres, E. Finocchio, G. Busca, E. Rodríguez-Castellón, J.L.G. Fierro, A. Jiménez-López, Micropor. Mesopor. Mater. 75 (2004) 23.
[35] J. Anderson, C. Fergusson, I. Rodriguez-Ramos, A. Guerrero-Ruiz, J. Catal. 192 (2000) 344.
[36] V. Hulea, E. Dumitriu, F. Patcas, R. Ropot, P. Graffin, P. Moreau, Appl. Catal. A: Gen. 170 (1998) 169.